

# The process of front-to-side collision of motor vehicles in terms of energy balance

Mirosław Gidlewski  · Leon Prochowski ·  
Leszek Jemioł · Dariusz Żardecki

Received: 7 June 2018 / Accepted: 28 November 2018 / Published online: 20 December 2018  
© The Author(s) 2018

**Abstract** The reconstruction of a road accident can be treated as the resolution of an “inverse problem” in mechanics using analytical or numerical models. In the road accident reconstruction research, an assumption is often made that a predominant part of the energy lost during vehicle collisions is consumed by permanent deformation of vehicle components. Other parts of the dissipated energy can be ignored due to their insignificant amount. In this article, this assumption will be verified for the front-to-side collision of passenger cars. The main objective of this paper is to determine the important components of the energy balance dissipated during the collision. These components were determined on the basis of experimental results, which included three crash tests with a front-to-side collision of motor vehicles of the same make and model, with the right-angle impact of one car against the side of another. The results of experiments were used to construct the model of the dynamics of the motor vehicle collision. The model was then used as a basis for the determination of the forces, displacements and velocities during vehicle collision. The above made it possible to determine vehicle force/deformation curves and then

the key components of the dissipated energy in function of the duration of the contact phase of the vehicle collision. Based on the results of the model and crash tests, conclusions were formulated that provide an important insight into the reconstruction of the front-to-side collisions of motor vehicles.

**Keywords** Cars’ collision dynamics · Collision energy balance

## 1 Introduction

The road accident analysis carried out by forensic experts is usually based on simplified methods and procedures due to a limited access to the numeric data necessary for computations. The reconstruction of the collision between two motor vehicles consists of the resolution of an “inverse problem” in mechanics, where the course of an accident is reconstructed, based on the accident description using appropriate analytical or simulation models derived from the principles of mechanics. When accident analyses and reconstructions are carried out in a standard way, i.e. without using the finite element method (FEM) or multi-body system dynamics (MBD), the calculations are based on discrete dynamic models of colliding objects. These models are supplemented by empirically determined force/deformation curves, vehicle parameters and empirical relations between the velocity of the impacting vehicle and the measured deformation of

M. Gidlewski (✉)  
Automotive Industry Institute (PIMOT), Warsaw, Poland  
e-mail: miroslaw.gidlewski@uthrad.pl

L. Prochowski · D. Żardecki  
Military University of Technology (WAT), Warsaw, Poland

M. Gidlewski · L. Jemioł  
University of Technology and Humanities in Radom, Radom,  
Poland

vehicle bodies [3, 11, 13–15, 17, 23], described with the use of energy rasters in a two- or three-dimensional meshed models.

Basic research addressed in [2, 5, 8, 26, 27] shows an immense amount of detailed scientific problems that are encountered when collisions are modelled and simulated even in relatively simple discrete systems. This is especially true when not only the impact-related phenomena but also the processes of energy dissipation due to frictional effects are to be taken into account. The introduction of dry friction with its singularities (Painlevé paradox, stick-slip processes, indeterminacy problems) fundamentally complicates the collision models and their analyses. As an example, if temporary bonds (nanoscale junctions) are to be taken into account, the Gauss principle must be used in the synthesis of the model, which will lead to extended mathematical descriptions even in seemingly simple cases [32]. Considering the experience from the analyses of nonlinear vibrations in discrete dynamic systems (“multi-rigid body systems” and “non-smooth systems”), where bifurcations and chaos are very frequent phenomena, the extended collision models directly derived from the laws of physics may be reasonably expected to show significant sensitivity. As a consequence of this sensitivity, and combined with the uncertainty of the data, the researchers who deal with the analysis and reconstruction of collisions in real systems are inclined to use simplified empirical formulas adapted for the processes to be examined.

In the area of applied research, there are many publications directly dedicated to motor vehicle collisions. They report crash test results, describe the techniques of measurements and the processing of signals and images recorded, and present simulation results obtained using software of the Multibody System Dynamics (MBD) type, e.g. MADYMO or the FEM type, e.g. LS-DYNA [9, 25]. A separate group of publications describes the accident reconstruction carried out using simplified analytical methods or specialized supporting software (e.g. CRASH) [4, 22, 28, 29]. In some research procedures, advanced signal processing and identification techniques are also used, as for example those based on the wavelet transformation and the NARMA method [18]. An extensive review of those approaches, together with examples of the application of experimental, analytical and simulation results to the analysis and reconstruction of motor vehicle collisions can be found, for example, in [1, 10, 21].

One of the basic methods in the analysis and reconstruction of motor vehicle collisions in the road traffic is the method of energy balance. The energy balance is compiled for all vehicles involved in the collision. The shares of individual components in the energy balance may vary and depend on the types and characteristics of the objects involved in the collision, and even on the specific scenario of the accident. In most cases, the raster methods used by experts (i.e. the methods based on the empirical relations between the velocity of the impacting vehicle and the vehicle body deformations along a simplified mesh model) reduce the energy balance to two main components, namely the pre-impact kinetic energy of the vehicles involved and the work carried out on the deformation of their bodies. The development of efficient methods to define also the remaining components of the energy balance, based on simple models and data recorded after the accident, is an objective of scientific research carried out at many research centres.

The methods and computational procedures concerning head-on vehicle collisions are relatively well explored, and the reconstruction of such accidents is often based on the dynamic 1D models or on the use of raster methods. Usually, an assumption is made that in the head-on collisions no lateral movement of the impacting vehicle takes place and, consequently, taking into account only two components of the energy balance is a correct hypothesis. These two components are the energy of the pre-impact translational motion and the energy of vehicle body deformation. Such hypothesis has been used to develop the methods of determining the impact velocity based on the vehicle body deformation depth (the Campbell method and the McHenry method). These methods are often used for accident analysis and reconstruction. As an example, they were used in [33] for the reconstruction of head-on collisions of several passenger cars with a barrier, and the accuracy of determining the pre-impact vehicle velocity was within twenty per cent. It was experimentally shown [19, 20] that even if the vehicle body deformation is of the order of 50 centimeters, the energy dissipated during a head-on collision can be roughly computed from the kinetic energy and the deformation raster by means of a linear equation, having the coefficient of restitution determined experimentally. An estimation of the energy dissipated for the deformation of colliding vehicles with significantly different masses has been presented in [12]. For the frontal impact against the side

of a stationary vehicle, the dissipated energy depends to a significant degree on the properties of the vehicle side body structure and on its previous repairs, if any [24]. The energy dissipation takes place both during the normal deformation and as a result of the relative movement of the vehicles, as will be further elaborated in this paper.

The front-to-side collisions, i.e. those taking place when a motor vehicle hits its front against the side of another vehicle, occur in a more complex way than the head-on collisions. In the front-to-side collisions, the process of destruction of vehicle bodies is accompanied by at least a 2D movement of the vehicles in relation to each other, and due to that the model becomes more complex. Limiting the energy balance to only two mentioned earlier components becomes unacceptable. Although the front-to-side collisions are quite frequent (in Poland, they constitute about 25% of all road accidents), their computer models are still relatively unexplored and, in consequence, it is challenging to analyse and reconstruct such scenarios.

The problems of energy balance and front-to-side collisions have been separately addressed in many publications dedicated to motor vehicle collisions. In the available literature, however, there is a lack of comprehensive and sufficiently in-depth analyses of these problems. Therefore, extending the area of energy analysis to the front-to-side collisions requires further experimental and modelling research. A justifiable question arises whether the description of these problems in a 2D space is adequate or rather a 3D model have to be build. As an example, even in the case of an almost completely planar (2D) but non-steady state motion, certain interactions take place as a result of the relative movements of the vehicles in the contact area during the collision. Does this disturbance affect considerably the accuracy of the accident reconstruction computations? The analysis of the available literature does not answer this question unequivocally due to the lack of comparative studies.

A few initial stages of the energy-based analysis of the front-to-side collision have already been presented by the authors in previous publications. Crash tests with about a dozen cars of the same make and model have been described in [6, 7]. In each test, the front of vehicle A impacted the left side of vehicle B. The velocity of vehicle A immediately before the collision was about 50 km/h, and it was twice as high as that of vehicle B. The procedure of determining the dynamic deforma-

tion of the vehicles taking part in the collision and some processes observed during the experiments have been presented.

This article reports on the progress in the search for an efficient method of analysis and reconstruction of the front-to-side collision of motor vehicles taking into account the process of energy dissipation resulting not only from the deformation of vehicle bodies but also from the fact that the cars slide on the road surface and move in relation to each other in the deformation zone (i.e. in the area of contact during the collision). The main objective of this paper is to determine the important components of the balance of the energy dissipated as a result of the collision and to show the variations of these components during the vehicle collision contact phase. In the road accident reconstruction research, an assumption is made that a predominant part of the energy lost during vehicle collisions is consumed by the permanent deformation of vehicle bodies, and the remaining parts of the dissipated energy can be ignored due to their insignificant value. In this paper, an attempt will be made to verify this assumption for the front-to-side collision of passenger cars, based on the results of crash tests and computer modelling. This article is an extension of the paper presented at the 14th International Conference “Dynamical Systems – Theory and Applications” DSTA 2017.

## 2 Experimental studies

Three crash tests were carried out at the Automotive Industry Institute (PIMOT) in Warsaw, involving six passenger cars of the same make and model. In each test, the front of car A was impacting the left side of car B, close to the B pillar (Fig. 1).

Cars A and B were loaded with measuring equipment and three test dummies: dummy Hybrid III at the driver’s seat, dummy Hybrid II at the front passenger’s seat, and the child dummy in the safety seat at the rear. All test dummies had appropriate seat belts fastened. The vehicles prepared for the crash tests were weighed and measured, with the position of the vehicle mass centre being determined as well. The moment of inertia of the vehicle with respect to the vertical axis passing through the vehicle mass centre was determined from an empirical formula [31]:

$$I_i = m_i L_{1i} L_{2i} \quad (1)$$

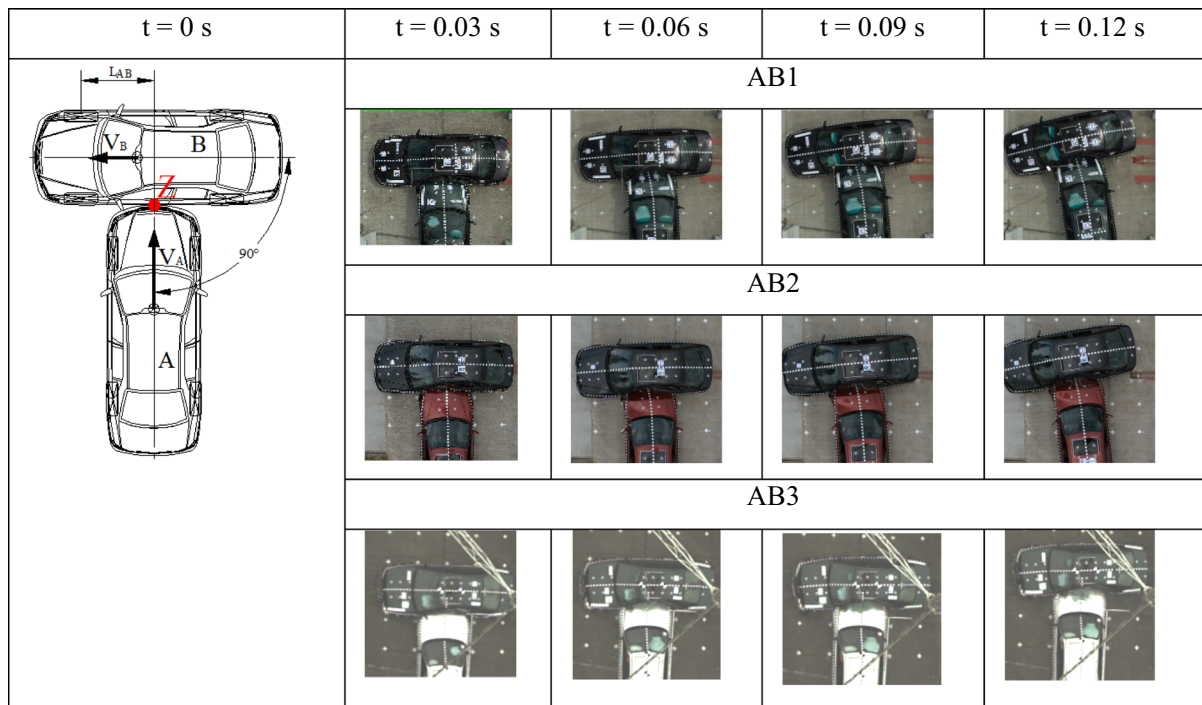


**Fig. 1** Relative positions of cars A and B during the collision

where  $L_{1i}$  and  $L_{2i}$ —distances between the vehicle mass centre and the front and rear vehicle axles, respectively (subscript “ $i$ ” indicates car A or B).

The moments of inertia of vehicle wheels were determined from the generally available data for passenger car wheels of the specific class. The relevant vehicle characteristics were as specified in Table 1.

The pre-impact velocity of car A was about 50 km/h. In the first two tests, vehicle B moved with a velocity half as high as that of vehicle A; during the third test, vehicle B was stationary. The location of the point of impact on the side of car B was defined by the distance  $L_{AB}$  between the longitudinal plane of symmetry of car A and the front wheel axis of car B. The values of the characteristic parameters of the cars have been specified in Table 1.

The crash tests were carried out at the PIMOT facility on a dry concrete surface. During the tests, the steering wheels of both cars were left free and their road wheels had no brakes applied. The tests were performed on Honda Accord cars manufactured between 2000 and 2002. The cars were in good technical condition and had undamaged and non-corroded bodies, which had not been previously repaired. At the cen-

tre of mass of each car, a three-axial accelerometer was installed, together with sensors for measuring the angular velocity components of the car body with respect to the three coordinate axes.

The data acquisition system used to record the acceleration and angular velocity components was placed in the car trunk, in the housing designed for vehicle crash tests. The vibro-isolating performance of such a housing was previously verified in separate tests. The sensor signals were subjected to a low-pass filtering. The signals were recorded with the use of a 10-kHz filter, and an additional filter with the cut-off frequency of 50 Hz was used at the final stage. That way the measured signals were reduced to the frequency band that can be reproduced in the modelling and equation-solving process. The filter cut-off frequency was selected after comparing with 100- and 25-Hz filters, to compromise between the expected calculation accuracy, interpretability of the calculation results, and the benefit of reaching conclusions that would be relevant and suitable for the modelling and reconstruction of road accidents of this type.

**Table 1** Vehicle characteristics

Description	AB1	AB2	AB3
Mass of car A, $m_A$ (kg)	1569	1532	1545
Mass of car B, $m_B$ (kg)	1568	1594	1629
Moment of inertia of car A, $I_A$ (kgm <sup>2</sup> )	2722	2636	2661
Moment of inertia of car B, $I_B$ (kgm <sup>2</sup> )	2710	2777	2827
$L_{AB}$ (m)	1.25	1.34	1.33
Velocity $V_A$ (m/s)	15.1	12.7	15.3

High-speed cameras were installed above the crash test location to record car positions with a frequency of 1000 frames per second.

### 3 Modelling of the collision

In order to analyse the processes that occur during the motor vehicle collision, the following coordinate systems were adopted:

- Local coordinate systems, fixed to the bodies of each of the “*i*” cars involved in the collision. The local coordinate system  $O_i x_i y_i z_i$  has its origin  $O_i$  situated at the centre of mass of the *i*th car and its  $O_i x_i$  axis is parallel to the car longitudinal centre-line. The signals recorded in the local coordinate systems were the components of the acceleration vector of the car mass centre ( $a_{xi}$ ,  $a_{yi}$ ,  $a_{zi}$ ) and of the angular velocity component ( $P_i$ ,  $Q_i$ ,  $R_i$ ) of the car.
- Local levelled coordinate systems, attached to the mass centres of each of the “*i*” cars. The local coordinate system  $O_i x_{Pi} y_{Pi} z_{Pi}$  has its origin  $O_i$  situated at the mass centre of the *i*th car, the  $O_i x_{Pi} y_{Pi}$  plane is parallel to the road surface, and the  $O_i x_{Pi}$  axis is parallel to the car longitudinal symmetry plane. The local levelled coordinate systems were used to formulate the equations of motion of the planar model of the collision.
- Global coordinate system  $O_G X_G Y_G Z_G$ , attached to the road. The  $O_G X_G Y_G$  plane of this system is situated at the road surface level and the  $O_G Z_G$  axis is pointing vertically upwards. The  $O_G X_G$  axis is parallel to the vector of pre-impact velocity of car A and the  $O_G Y_G$  axis is parallel to the vector of pre-impact velocity of car B. In the global coordinate system, the time histories of the translational

and rotational velocities, and the trajectories of the involved cars were determined.

The measurements obtained in the local coordinate systems were transformed to other coordinate systems. The rotation of the local systems with respect to the global coordinate system is defined by angles  $\Phi_i$  (vehicle roll angle),  $\Theta_i$  (vehicle pitch angle) and  $\Psi_i$  (vehicle yaw angle).

The angular velocity components of the car body in the global coordinate system are described as follows:

$$\begin{bmatrix} \dot{\Phi}_i \\ \dot{\Theta}_i \\ \dot{\Psi}_i \end{bmatrix} = \begin{bmatrix} 1 & \sin \Phi_i \operatorname{tg} \Theta_i & \cos \Phi_i \operatorname{tg} \Theta_i \\ 0 & \cos \Phi_i & -\sin \Phi_i \\ 0 & \frac{\sin \Phi_i}{\sin \Theta_i} & \frac{\cos \Phi_i}{\cos \Theta_i} \end{bmatrix} \cdot \begin{bmatrix} P_i \\ Q_i \\ R_i \end{bmatrix} \quad (2)$$

The acceleration of the car mass centre in the levelled coordinate system is expressed by the following formula:

$$\begin{bmatrix} a_{xPi} \\ a_{yPi} \\ a_{zPi} \end{bmatrix} = \begin{bmatrix} \cos \Theta_i & \sin \Theta_i \sin \Phi_i & \sin \Theta_i \cos \Phi_i \\ 0 & \cos \Phi_i & -\sin \Phi_i \\ -\sin \Theta_i & \cos \Theta_i \sin \Phi_i & \cos \Theta_i \cos \Phi_i \end{bmatrix} \times \begin{bmatrix} a_{xi} \\ a_{yi} \\ a_{zi} \end{bmatrix} \quad (3)$$

The acceleration components of the mass centres of individual cars, expressed in the global coordinate system, are described by formulas:

$$\begin{bmatrix} \ddot{X}_{GA} \\ \ddot{Y}_{GA} \\ \ddot{Z}_{GA} \end{bmatrix} = \begin{bmatrix} \cos \Psi_A & -\sin \Psi_A & 0 \\ \sin \Psi_A & \cos \Psi_A & 0 \\ 0 & 0 & 1 \end{bmatrix} \begin{bmatrix} a_{xPA} \\ a_{yPA} \\ a_{zPA} \end{bmatrix} \quad (4)$$

$$\begin{bmatrix} \ddot{X}_{GB} \\ \ddot{Y}_{GB} \\ \ddot{Z}_{GB} \end{bmatrix} = \begin{bmatrix} \cos(90^\circ + \Psi_B) & -\sin(90^\circ + \Psi_B) & 0 \\ \sin(90^\circ + \Psi_B) & \cos(90^\circ + \Psi_B) & 0 \\ 0 & 0 & 1 \end{bmatrix} \times \begin{bmatrix} a_{xPB} \\ a_{yPB} \\ a_{zPB} \end{bmatrix} \quad (5)$$

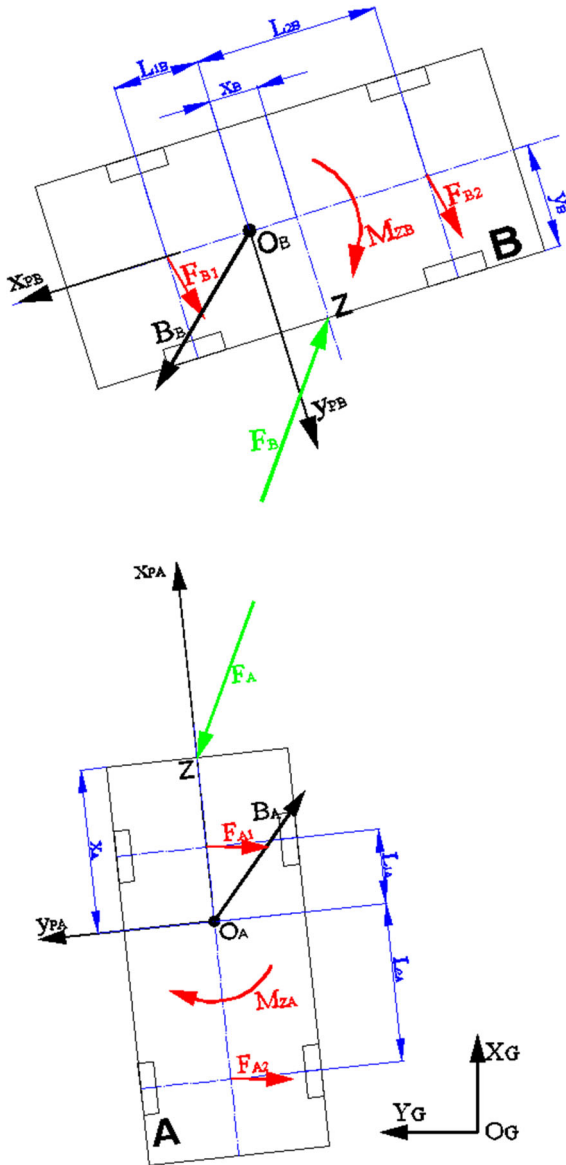


**Fig. 2** Coordinate systems, key dimensions and the location of the impact force vector

The process of dissipation of the impact energy was analysed using a planar model of the dynamics of the motor vehicle collision, with the forces and moments acting on the cars during the collision expressed in the local levelled coordinate systems (Fig. 2). The equations of motion (6) of cars A and B were based on the equations of the equilibrium of forces and moments that act on cars A and B in the corresponding levelled coordinate systems.

$$\begin{cases}
 m_A \cdot a_{xPA} = F_{xA} + F_{xA1} + F_{xA2} \\
 m_A \cdot a_{yPA} = F_{yA} + F_{yA1} + F_{yA2} \\
 I_A \cdot \ddot{\Psi}_A \\
 = F_{yA} \cdot x_A - F_{xA} \cdot y_A + F_{yA1} \cdot L_{1A} + F_{yA2} \cdot L_{2A} \\
 m_B \cdot a_{xPB} = F_{xB} + F_{xB1} + F_{xB2} \\
 m_B \cdot a_{yPB} = F_{yB} + F_{yB1} + F_{yB2} \\
 I_B \cdot \ddot{\Psi}_B \\
 = F_{yB} \cdot x_B - F_{xB} \cdot y_B + F_{yB1} \cdot L_{1B} + F_{yB2} \cdot L_{2B} \\
 F_{yB} = -F_{xA} \cdot \cos \gamma_{AB} + F_{sA} \cdot \sin \gamma_{AB} \\
 F_{xB} = -F_{xA} \cdot \sin \gamma_{AB} - F_{yA} \cdot \cos \gamma_{AB}
 \end{cases} \quad (6)$$

where

- $B_i (B_{ix}, B_{iy})$  inertial force acting on the  $i$ th car, expressed in the levelled coordinate system attached to the mass centre of the car;
- $M_{zi}$  moment of the inertial resistance acting on the car during its accelerated rotation around the vertical axis;
- $m_i, I_i$  vehicle mass and mass moment of inertia of the car relative to the vertical axis;
- $a_{xPi}, a_{yPi}$  longitudinal and lateral components of the acceleration vector of the centre of car mass, calculated from (3);
- $F_{i1}(F_{xi1}, F_{yi1})$  tangent road reaction force acting on the wheels of the front car axle and its components; and similarly
- $F_{i2}(F_{xi2}, F_{yi2})$  tangent road reaction force acting on the wheels of the rear car axle and its components, expressed in both cases in the levelled coordinate system attached to the centre of mass of the  $i$ th car;
- $F_i(F_{xi}, F_{yi})$  impact force acting on the vehicle and the longitudinal ( $x$ ) and lateral ( $y$ ) components of this force, expressed in the levelled coordinate system attached to the mass centre of the  $i$ th car;
- $x_i, y_i$  coordinates of point Z, i.e. the point of application of the impact force, in the levelled coordinate system attached to the mass centre of the  $i$ th car (Fig. 2);

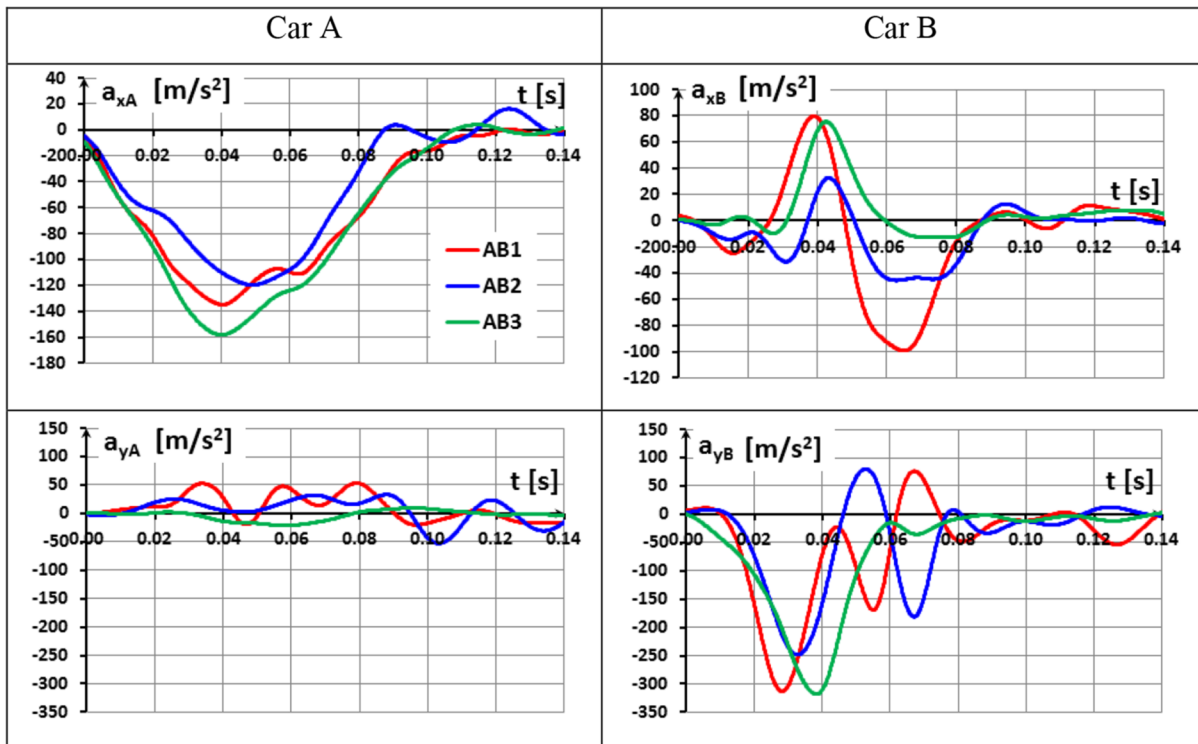


**Fig. 3** Components (longitudinal  $a_{xi}$  and lateral  $a_{yi}$ ) of the accelerations of mass centres of cars A and B in the local coordinate systems  $O_i x_i y_i z_i$

$\gamma_{AB}$  angle of rotation of vehicle B around the vertical axis (car B yaw angle), measured from the longitudinal symmetry plane of vehicle A ( $\gamma_{AB} = \Psi_A - \Psi_B$ ).

This way, a system of six differential equations with respect to the coordinates defining the positions of the mass centres and rotations of cars A and B was obtained (6), comprising also two algebraic equations. This system will be treated as a system of solely algebraic equations, because the time histories of components of the vector of translational acceleration of the mass centres and of the vectors of angular acceleration of the cars are known. They were calculated from the experimental results with the time step of  $\Delta t = 0.0001$  s, by converting the measurement results to the levelled coordinate systems using relation (3). Therefore, the unknowns in Eq. (6) are components  $F_{xA}, F_{yA}, F_{xB}, F_{yB}$  of the impact force and the lateral reaction forces  $F_{yA1}, F_{yA2}, F_{yB1}, F_{yB2}$  acting on car wheels.

#### 4 Experimental studies and modelling results

Selected measurements of accelerations are shown in Fig. 3. They represent the longitudinal  $a_{xi}$  and lateral  $a_{yi}$  components of the accelerations of the mass centres of cars A and B in the local coordinate systems after applying the 50-Hz filter.

Based on the photogrammetric analysis of high-speed camera images, discrete values of the car body marker displacements during the crash tests were determined. Then, these values were used to determine the displacements of the centres of mass and yaw angles of cars A and B bodies with the sampling step of  $\Delta t = 0.01$  s. The determined values were plotted as points in Fig. 6, together with curves representing calculation results. This comparison confirms that the calculation results are correct. The small differences between the results thus juxtaposed can be explained by a relatively low accuracy of determining the marker positions in subsequent frames of the video recordings.

An analysis was carried out for the time histories of selected quantities extending for the time period from

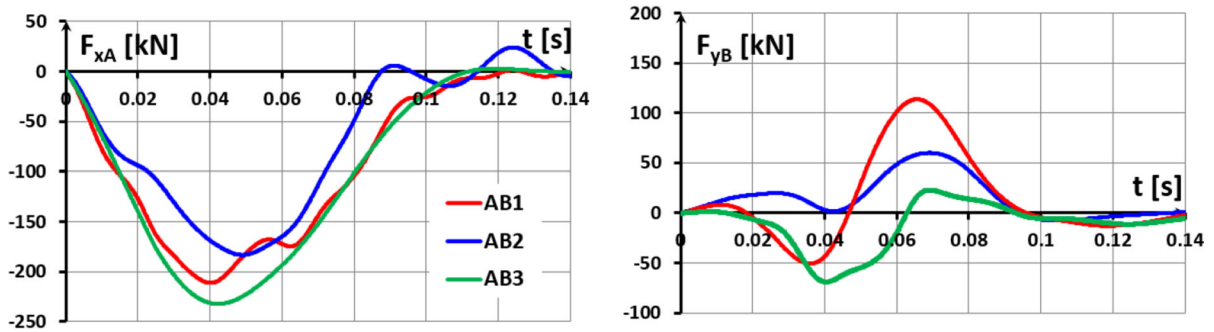


**Fig. 4** Longitudinal component  $F_{xA}$  of the impact force exerted by car A and the lateral component  $F_{yB}$  of the vector of the impact force exerted by car B

the instant when car A came into contact with car B, i.e. from  $t = 0$  s, to  $t = 0.14$  s. During this period, the following phases of the experiment were observed (Fig. 1):

- Collision of the cars and their temporary contact (with the compression phase followed by the restitution phase);
- Separation of the cars;
- Start of the independent post-separation movements of the cars.

Figure 4 shows the longitudinal component  $F_{xA}$  of the impact force exerted by car A and in the lateral component  $F_{yB}$  of the impact force exerted by car B. They were computed from the system of Eq. (6). The longitudinal component  $F_{xA}$  will be used to determine the work carried out for the deformation of the front of car A and the side of car B. The lateral component  $F_{yB}$  of the impact force will be used to determine the work of frictional forces done when the vehicle bodies move against each other in the contact area. An analysis of the curves representing the components of the impact force in Fig. 4 made it possible to identify the instant at which cars A and B came out of contact with each other. The vehicle separation has been assumed to take place when the longitudinal force component  $F_{xA}$  reached zero. After that, the vehicles moved independently. In tests AB1, AB2, and AB3 (Table 1), the vehicles were separated at times  $t_k = 0.12$  s,  $t_k = 0.09$  s, and  $t_k = 0.11$  s, respectively. The time instants thus identified are necessary to calculate the values of the translational and rotational velocities of the cars, as well as to determine the position of the cars in relation to each other and to the road when they separate.

It is worth noticing that the maximum value of the longitudinal component of the impact force  $F_{xA}$  in test AB2 was markedly lower than in the other two tests. The reason for this is the lower value of the impact velocity recorded in test AB2. Another factor having an influence on the impact force curves is the distance between the impact point (point Z in Fig. 2) and the mass centre of car B (Table 1).

Figure 5 shows experimental test and calculation results after the transformation of the measurement results to the global coordinate system. The curves represent the time histories of translational velocities  $V_{wA}$  and  $V_{wB}$  of the mass centres of cars A and B and the angular velocities  $\dot{\Psi}_A$  and  $\dot{\Psi}_B$  of these cars around the vertical axis, calculated according to (2). The translational velocities were determined from (7), with the velocity vector components having been previously calculated by numerical integration with respect to time (by the trapezoidal rule) of components  $\ddot{X}_{Gi}$  and  $\ddot{Y}_{Gi}$  of the acceleration vectors of the car mass centres according to (4) and (5). The curves in Fig. 5 show relevant quantities needed to calculate the dissipated energy. The vehicle velocities determined from the equation

$$V_{wi} = \sqrt{\dot{X}_{Gi}^2 + \dot{Y}_{Gi}^2} \quad (7)$$

were used to calculate the kinetic energy of the vehicles during the vehicle contact phase.

Changes in the positions of cars A and B during the compression and restitution phases have been shown in Fig. 6. The motion has been described with the use of three quantities, namely the longitudinal and lateral displacements of the car mass centres ( $X_{Gi}$  and  $Y_{Gi}$ ) and vehicle body yaw angles  $\Psi_i$ . The axes of the coordinate systems  $O_{Gi}X_{Gi}Y_{Gi}Z_{Gi}$  are parallel to those of



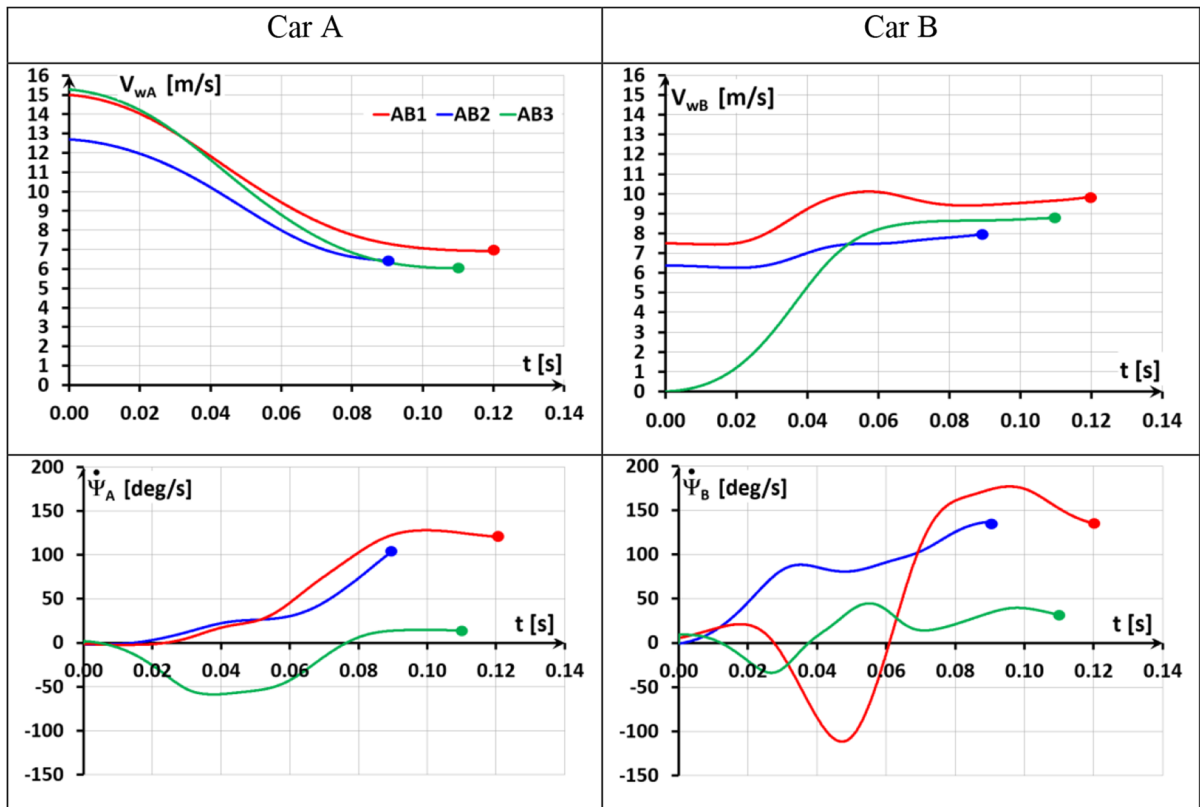


**Fig. 5** Time histories of translational velocities  $V_{wA}$  and  $V_{wB}$  of the centres of mass of cars A and B and angular velocities  $\dot{\Psi}_A$  and  $\dot{\Psi}_B$  of the car bodies during the contact phase of vehicle collision

the global coordinate system and their origins (points  $O_{Gi}$ ) coincide with the positions of the mass centres of the respective ( $i$ th) car at the beginning of contact between the vehicles. It is noteworthy that during the collision, the longitudinal centrelines of cars A and B only slightly deviated from their pre-impact positions. At the time instant  $t_k$ , the yaw angle  $\Psi_A$  of car A did not exceed  $5^\circ$  and the yaw angle  $\Psi_B$  of car B was less than  $7^\circ$ . Therefore, the cars during the contact phase were situated with respect to each other at the angle almost identical to the initial state ( $t = 0$  s). This finding was utilized to determine the combined deformation of both cars, assuming that the deformation progressed in the direction defined by the longitudinal centreline of car A. This means that the calculations described above are essential for the presented analysis.

It has been noticed that integrating the results of acceleration and angular velocity measurements may result in errors even at a small zero calibration error of the individual sensors before the crash test. Therefore,

the results of the calculations shown in Fig. 6, obtained by numerical integration of expressions (2), (4) and (5), were verified by comparing them with the results of a frame-by-frame analysis of the video recordings acquired from the camera installed above the crash test location (Fig. 6). Sensor calibration corrections introduced afterwards allowed to achieve a good consistency between the calculated positions of the car contours on the road and the actual vehicle positions on the road during the crash test. Exemplary comparison of the results has been shown in Fig. 7.

Based on the knowledge of the time histories of coordinates  $O_i(X_{Gi}, Y_{Gi})$  of the mass centres of each of the “ $i$ ” cars involved in the collision in the horizontal plane of the global coordinate system  $O_G X_G Y_G Z_G$ , and of the time histories of yaw angles  $\Psi_i$  of each car bodies, equations of straight lines going through the points  $O_A$  and  $O_B$  and coinciding with the longitudinal car centrelines at any instant during the contact phase of the collision can be determined (Fig. 8).

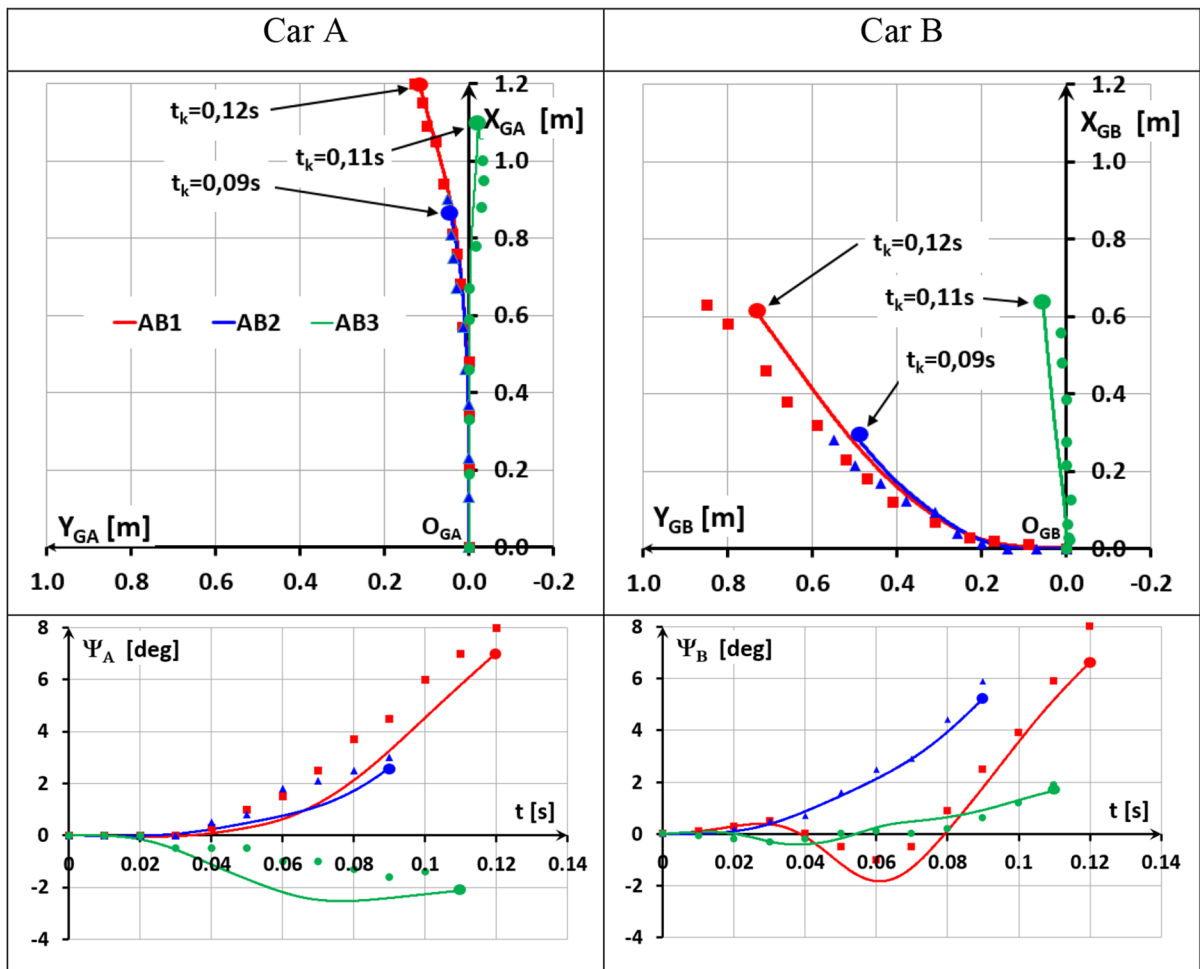


**Fig. 6** Displacements of the mass centres of cars A and B in the coordinate system  $O_{Gi}X_{Gi}Y_{Gi}Z_{Gi}$  and yaw angles  $\Psi_i$  (angles of rotation around the vertical axis) of both cars during the contact

phase of vehicle collision (the solid lines represent calculation results; the points represent results of a frame-by-frame analysis of the video recordings acquired from the high-speed cameras)

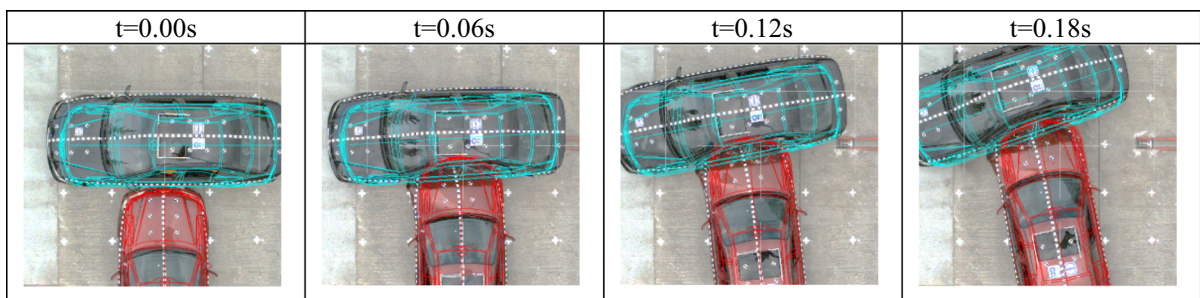


**Fig. 7** Calculated positions of car contours on the road against the background of the recorded frames (test AB2)

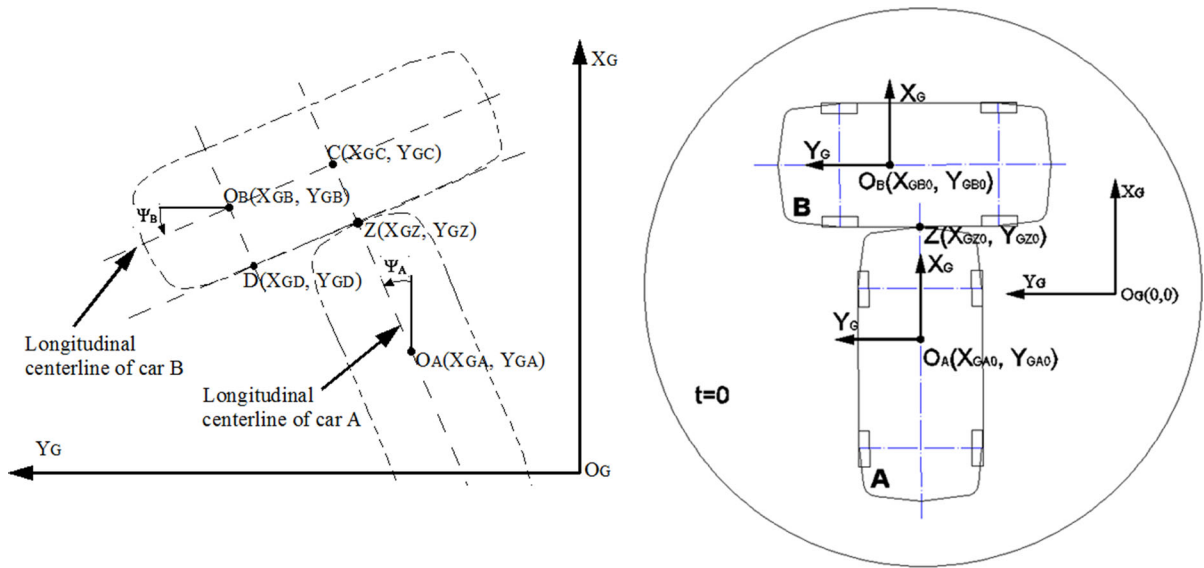


**Fig. 8** Determination of the deformation of the front of car A and the side of car B, and the displacement along which the work is done by the friction force between the cars during the collision

The intersection of these lines defines the coordinates of the point  $C(X_{GC}, Y_{GC})$  as follows:

$$X_{GC} = \frac{(\operatorname{tg}(\frac{\pi}{2} - \Psi_A) \cdot Y_{GA} - X_{GA}) \operatorname{tg}(-\Psi_B) - (\operatorname{tg}(-\Psi_B) \cdot Y_{GB} - X_{GB}) \operatorname{tg}(\frac{\pi}{2} - \Psi_A)}{\operatorname{tg}(\frac{\pi}{2} - \Psi_A) - \operatorname{tg}(-\Psi_B)} \tag{8}$$

$$Y_{GC} = \frac{(\operatorname{tg}(\frac{\pi}{2} - \Psi_A) \cdot Y_{GA} - X_{GA}) - (\operatorname{tg}(-\Psi_B) \cdot Y_{GB} - X_{GB})}{\operatorname{tg}(\frac{\pi}{2} - \Psi_A) - \operatorname{tg}(-\Psi_B)} \tag{9}$$

The centre of mass  $O_A$  of car A and the point C define a line segment  $O_A C$  (Fig. 8), the length of which is:

$$O_A C = \sqrt{(X_{GC} - X_{GA})^2 + (Y_{GC} - Y_{GA})^2} \tag{10}$$

The change in the length of the line segment  $O_A C$  during the contact phase of the collision makes it possible to determine the combined deformation  $c_A$  of the front of car A and the side of car B:

$$c_A = O_A C^0 - O_A C \tag{11}$$

where

$O_A C^0$  length of the line segment  $O_A C$  at the beginning of the collision phase ( $t = 0$  s).

Point Z is a hypothetical point of contact of the front of car A with the side of car B (Figs. 2, 8) and, simultaneously, the point of application of the impact force.

An assumption was made that the point Z constantly lies in the longitudinal centreline of car A and is coming closer to point  $O_A$  with the increasing deformation of

the front of car A. Hence, the distance between points Z and  $O_A$  is:

$$O_A Z = c_A - \frac{F_{nA}}{K} \tag{12}$$

where

$K$  average stiffness coefficient of the front of car A approximated from the deformation characteristics [16].

The coordinates of point Z in the global coordinate system are described by formulas

$$X_{GZ} = X_{GA} + O_A Z \cdot \cos \Psi_A \tag{13}$$

$$Y_{GZ} = Y_{GA} + O_A Z \cdot \sin \Psi_A \tag{14}$$

Point D ( $X_{GD}, Y_{GD}$ ) in Fig. 8 is defined as the intersection of the straight line going through point Z and parallel to the longitudinal centreline of car B with

the straight line going through point  $O_B$  and perpendicular to the longitudinal centreline of car B. In the global coordinate system, the coordinates of point D are described by equations:

$$X_{GD} = \frac{(\operatorname{tg}(\frac{\pi}{2} - \Psi_B) \cdot Y_{GB} - X_{GB}) \operatorname{tg}(\pi - \Psi_B) + (\operatorname{tg} \Psi_B \cdot Y_{GZ} + X_{GZ}) \operatorname{tg}(\frac{\pi}{2} - \Psi_A)}{\operatorname{tg} \Psi_B + \operatorname{tg}(\frac{\pi}{2} - \Psi_B)} \quad (15)$$

$$Y_{GD} = \frac{(X_{GZ} + \operatorname{tg} \Psi_B \cdot Y_{GZ}) - (X_{GB} - \operatorname{tg}(\frac{\pi}{2} - \Psi_B) \cdot Y_{GB})}{\operatorname{tg} \Psi_B + \operatorname{tg}(\frac{\pi}{2} - \Psi_B)} \quad (16)$$

It has been assumed that the front of car A moves in relation to the side of car B along the straight line passing through the points Z and D (Fig. 8).

The length of the line segment ZD is defined by the formula:

$$ZD = \sqrt{(X_{GD} - X_{GZ})^2 + (Y_{GD} - Y_{GZ})^2} \quad (17)$$

The displacement  $c_B$  along which the frictional force between the vehicles is acting when the vehicle bodies slide on each other is described by the formula:

$$c_B = ZD^0 - ZD \quad (18)$$

where

$ZD^0$  length of the segment ZD at the time instant  $t = 0$ .

The combined deformation  $c_A(t)$  of the front of car A and the side of car B during the contact phase of the vehicle collision has been shown in Fig. 9a. This deformation, measured along the longitudinal centreline of car A, increases during the compression phase, which lasts until the maximum value  $c_{Amax}(t_m)$  is reached. The deformation then decreases (during the restitution phase) to reach the value of  $c_R(t_k)$  at the time of vehicle separation. The displacement  $c_B(t)$  of the front of car A on the side of car B during the contact phase of the vehicle collision has been shown in Fig. 9b. The value of this displacement rapidly increases during the compression phase and the rate of this growth markedly drops during the restitution phase.

Based on the results of the calculations of  $F_{nA}(t)$  and  $c_A(t)$ , the force vs deformation curve was plotted for the combined deformation of the front of car A and the side of car B that occurred during the contact phase of the collision (Fig. 10a). Also, using the results of the calculations of  $F_{xB}(t)$  and  $c_B(t)$ , a curve was plotted

that characterizes the friction between the front of car A and the side of car B (Fig. 10b). The area between the deformation curve and the horizontal axis represents the energy consumed for the deformation of the front of car A and the side of car B, while the area under the

friction force curve represents the work done by this force when the vehicle bodies slide against each other in the contact area between them.

## 5 Basic energy components involved in the energy dissipation process

The energy dissipation process takes place during the contact phase of the collision and during the post-impact vehicle movements. The following energy components can be discerned as being involved in the contact phase of the collision:

- Initial kinetic energy of the vehicles, determined by their pre-impact translational motion and rotational motion of vehicle wheels and rotating components of the powertrain;
- Deformation work of vehicle bodies in their contact zone;
- Friction work done when the vehicle bodies slide against each other in the contact area between them;
- Work related to the displacement of vehicles in their translational and rotational motion;
- Energy dissipated in the vehicles suspensions and tyres;
- Thermal and vibrational energy released as a result of deformations and processes of destruction of vehicle components.

The kinetic energy of the car at the beginning of the impact phase (the initial kinetic energy) was calculated as a sum of the kinetic energy of the translational motion of the car mass and the rotational motion of components of the powertrain and the drive system of the car. The rotational velocity of the wheels and the parts connected with them is determined at every time

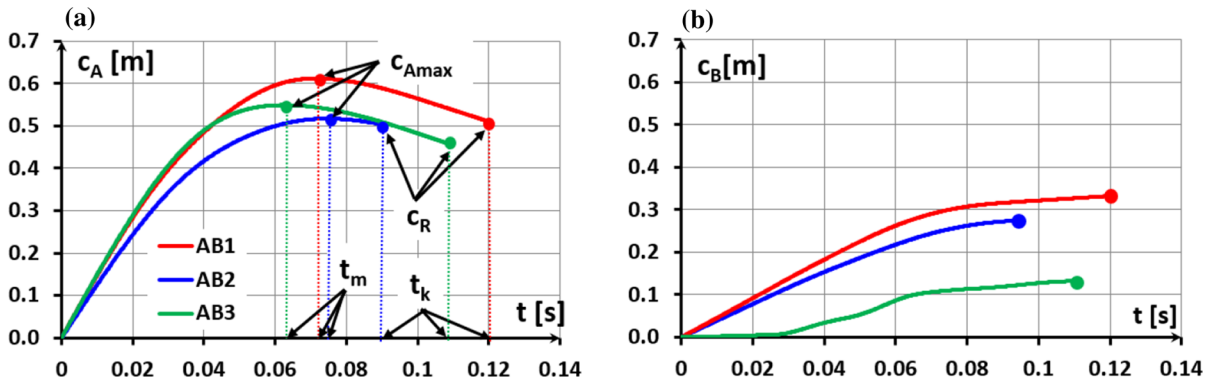


Fig. 9 Combined deformation  $c_A$  of the front of car A and the side of car B and the displacement  $c_B$  along the action of the frictional force between the cars during the contact phase of the collision

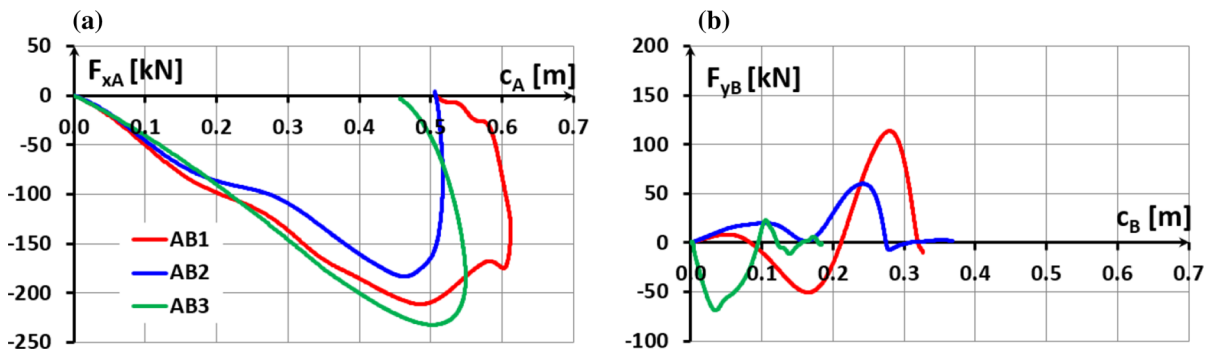


Fig. 10 Combined deformation of the front of car A and the side of car B and the friction force between the cars during the contact phase of the collision

instant by the velocity of the translational motion of the car body. Note that the road wheels of the cars were not braked during the tests. During the collision, the energy dissipation also occurs at the wheels (tyre deformation, friction forces in the tyre–road contact area, longitudinal and lateral slip of the tyres). The work done by the tyre–road friction forces and the dissipation of the kinetic energy of the wheels with decreasing directional velocity of the vehicle body were taken into account in the calculations.

Each component of the dissipated energy is a time series  $X(t_j)$  with a time step of  $\Delta t$ . Time  $t_j$  is described by the following expression:

$$t_j \in (t_0, t_1, t_2, \dots, t_m, \dots, t_k) \tag{19}$$

The change in the kinetic energy  $E_{ki}(t_j)$  of the  $i$ th vehicle during the collision is described by the equation:

$$E_{ki}(t_j) = \frac{m_i \cdot V_{wi}^2(t_j)}{2} + \frac{I_i \cdot \dot{\Psi}_i^2(t_j)}{2}$$

$$+ \frac{(I_{kp} + I_{kt}) \cdot \omega_{ki}^2(t_j)}{2} \tag{20}$$

where

$I_{kp}$  moment of inertia of the front wheels and rotating components of the powertrain;

$I_{kt}$  moment of inertia of the rear wheels;

$\omega_{ki}$  angular velocity of the wheels of the  $i$ th vehicle.

The total kinetic energy  $E_{kAB}$  of cars A and B during collision is:

$$E_{kAB}(t_j) = E_{kA}(t_j) + E_{kB}(t_j) \tag{21}$$

The deformation work  $E_D(t_j)$  of the front of car A and the side of car B during the contact phase of the collision is expressed by the following equations.

For  $t_j \leq t_m$  (Fig. 9):

$$E_D(t_j) = E_D(t_{j-1}) + \frac{[F_{xA}(t_j) + F_{xA}(t_{j-1})]}{2} \times [c_A(t_j) - c_A(t_{j-1})] \tag{22}$$

For  $t_m < t_j \leq t_k$  (rys. 9):

$$E_D(t_j) = E_D(t_m) - \left\{ E_D(t_{j-1}) + \frac{[F_{xA}(t_j) + F_{xA}(t_{j-1})]}{2} \times [c_A(t_j) - c_A(t_{j-1})] \right\} \quad (23)$$

The friction work  $E_T(t_j)$  occurring when the front of car A slides against the side of car B during the contact phase of the collision is expressed by equation:

$$E_T(t_j) = E_T(t_{j-1}) + \frac{|F_{xB}(t_j) + F_{xB}(t_{j-1})|}{2} \times [(c_B(t_j) - c_B(t_{j-1}))] \quad (24)$$

The friction work  $E_{Ti}(t_j)$  occurring when the  $i$ th vehicle wheels slide against the road surface is described as follows:

$$E_{Ti}(t_j) = E_{Ti}(t_{j-1}) + \frac{|F_{yi1}(t_j) + F_{yi1}(t_{j-1})|}{2} \times [(s_{i1}(t_j) - s_{i1}(t_{j-1}))] + \frac{|F_{yi2}(t_j) + F_{yi2}(t_{j-1})|}{2} \times [(s_{i2}(t_j) - s_{i2}(t_{j-1}))] \quad (25)$$

where

$s_{i1}$  lateral displacement of the front wheels of the  $i$ th vehicle during the contact phase of the collision;

$s_{i2}$  lateral displacement of the rear wheels of the  $i$ th vehicle during the contact phase of the collision.

The total friction work occurring when the wheels of car A and car B slide against the road surface is:

$$E_{tAB}(t_j) = E_{tA}(t_j) + E_{tB}(t_j) \quad (26)$$

The remaining energy lost during the contact phase of the collision is defined as shown below:

$$E_p(t = t_k) = E_{kAB}(t = 0) - [E_{kAB}(t = t_k) + E_D(t = t_k) + E_T(t = t_k) + E_{tAB}(t = t_k)] \quad (27)$$

Equations (19)–(26) were used to determine the variation of individual energy components during the contact phase of the vehicle collision. Fig. 11 shows the time histories of the kinetic energy of car A ( $E_{kA}$ ) and car B ( $E_{kB}$ ), work of deformation ( $E_D$ ) of vehicle bodies in their contact zone, friction work ( $E_T$ ) occurring when the vehicle bodies slide against each other, and

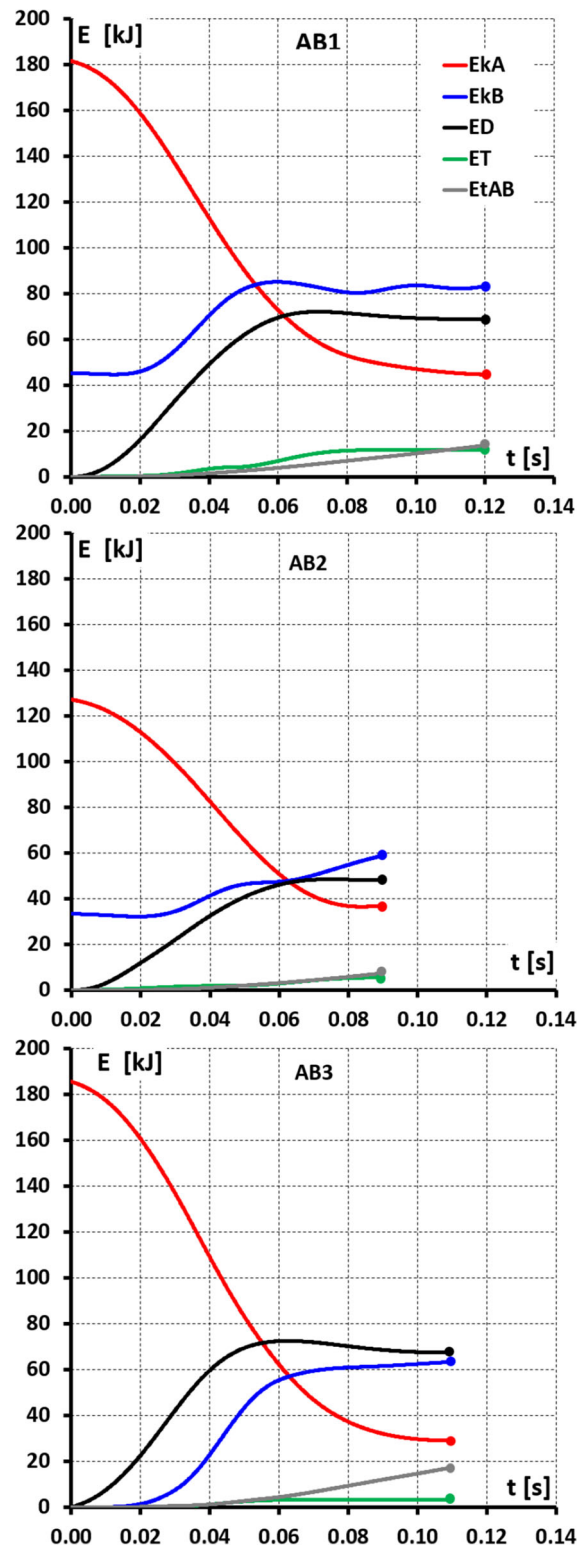


Fig. 11 Variation of the individual energy components during the contact phase of the collision in tests AB1, AB2 and AB3

**Table 2** Values of individual components of the energy balance

	Test AB1	Test AB2	Test AB3		Test AB1	Test AB2	Test AB3
$E_{kAB}(t = 0)$ (kJ)	226.9	160.5	185.5	$E_{kAB}(t = 0)$ (%)	100	100	100
$E_{kAB}(t = t_k)$ (kJ)	128.0	95.9	92.4	$E_{kAB}(t = t_k)$ (%)	56.4	59.8	49.8
$E_D(t = t_k)$ (kJ)	68.9	48.3	67.4	$E_D(t = t_k)$ (%)	30.3	30.1	36.3
$E_T(t = t_k)$ (kJ)	11.9	5.5	3.4	$E_T(t = t_k)$ (%)	5.2	3.4	1.8
$E_{tAB}(t = t_k)$ (kJ)	13.8	7.4	17.3	$E_{tAB}(t = t_k)$ (%)	6.1	4.6	9.4
$E_p(t = t_k)$ (kJ)	4.4	3.4	4.9	$E_p(t = t_k)$ (kJ)	2.0	2.1	2.7

work related to the vehicles displacement in their translational and rotational motion ( $E_{tAB}$ ).

The values of the considered energy components at characteristic time instants during the contact phase of the collision are listed in Table 2.

Table 2 shows that during the contact phase of the collision under consideration, the cars incurred the loss of 40.2–50.2% of their initial energy. Among the energy lost, the work used for vehicle deformation takes merely 70–75%. This finding shows an important difference between the front-to-side collisions and the head-on collisions of passenger cars, as practically all the initial energy is consumed by vehicle deformation during the contact phase in the latter case. The research presented in this paper has shown that in the case of the front-to-side collisions, the energy dissipated is also consumed by such phenomena as, for example, the friction between the vehicles involved, and the friction between the tyres and the road during their lateral displacement. This part of the energy lost should not be ignored in the calculations carried out during the reconstruction of the front-to-side collisions of motor vehicles. In order to verify the influence of this component of the energy balance on the result of calculations of the pre-impact velocity of car A, calculations based on the following equation were made [21]:

$$\Delta E = 0.5 \cdot (1 - k^2) \frac{m_A m_B}{m_A + m_B} (V_A - V_B)^2 \tag{28}$$

where  $\Delta E$ , energy lost during the collision;  $k$ , coefficient of restitution;  $V_A$ ,  $V_B$ , pre-impact velocity of the cars.

Equation (28) is used for the analysis of head-on car collisions, for which it was derived. After adopting certain assumptions, an attempt was made to use this formula for the front-to-side (right-angle) collision. For the computations, it was assumed that the only significant changes occur in the values of the lon-

gitudinal component of the pre-impact velocity of car A (impacting car B with its front) and the values of the lateral component of the velocity of car B (which was struck on its side). Any potential changes in the values of the remaining components of the velocity vectors of cars A and B were ignored. With the above described assumptions, Eq. (28) can be written in the following form:

$$V_A = \sqrt{\frac{2 \cdot \Delta E \cdot (m_A + m_B)}{(1 - k^2) \cdot m_A m_B}} \tag{29}$$

The pre-impact velocity  $V_A$  of car A was calculated from formula (28) (Table 3), with the ( $E_D + E_T + E_{tAB} + E_p$ ) and  $E_D$  energy values being substituted in turn for  $\Delta E$ . The value of the coefficient of restitution, necessary for the calculations, was determined from separate experimental results.

The calculation results presented in Table 3 are an example of using the energy balance of the front-to-side motor car collision. They are showing that using the car body deformation work during the collisions of this type, which often happens for the accident reconstruction purposes, results in underestimating the velocity of the impacting car by 11–14%.

## 6 Summary and conclusions

In the paper, the energy dissipation process and energy components during the front-to-side vehicle collision were determined on the basis of:

- Measurements carried out during motor vehicle crash tests;
- Calculations of the forces, velocities and displacements in the car contact zone, based on the model of the motor vehicle collision dynamics;

**Table 3** Pre-impact velocity of car A, obtained from the experiment and as computed

Velocity of car A (m/s)	AB1	AB2	AB3
$V_A$ (experiment)	15.1	12.7	15.3
$V_A$ (calculated for $\Delta E = E_D + E_T + E_{tAB} + E_p$ )	15.9	13.0	15.4
$V_A$ (calculated for $\Delta E = E_D$ )	13.4	11.3	13.2

- Verification of car positions by means of a frame-by-frame analysis of the video recordings of the experiments.

The results of experiments and model computations made it possible to determine important elements in the process of the energy dissipation during the front-to-side motor vehicle collision. The presence of the compression and restitution phases during the contact phase of the collision was taken into account. The following conclusions were formulated that enhance the existing approach for the reconstruction of the front-to-side collision of passenger cars (an impact at a right angle against a moving or stationary car):

1. It has been confirmed that the Eq. (29) can be useful for the calculation of the impacting car's velocity in the front-to-side collisions of passenger cars if some necessary initial assumptions are made. Also, it has been found that the value of the lost energy  $\Delta E$  should be taken higher by about 25–30% than the energy calculated from the post-impact vehicle deformation.
2. It has been pointed out that the work of deformation of the front and side parts of the cars makes about 70–75% of the total energy lost (Table 2) by the vehicles during the contact phase of the collision and that this percentage is definitely lower than that observed in head-on car collisions.
3. During the right-angle collision, the vehicles involved remain in a practically unchanged position relative to each other for the entire duration of the contact phase of the collision ( $t_k = 0.09 - 0.12$  s, Fig. 1), in spite of their translational and rotational motion during that period (Figs. 6, 7). Identical findings have been presented in [30]. This fact considerably facilitates the interpretation of the measurement results obtained from the experiments, at least for the central impact locations of certain range.
4. The impact against a motionless vehicle differs from a similar impact against a vehicle in motion in

that far less energy is lost in the former case due to friction between the vehicle bodies sliding on each other and, on the other hand, much more energy is used for the translation and rotation of the vehicles on the road surface during the contact phase of the collision.

The calculation results presented in Table 3 have shown that the method of combined analysis of experiment and modelling results, as used here to determine individual components of the energy balance during the contact phase of vehicle collision, provides the opportunity for a significant improvement in the accuracy of the process of reconstruction of complex road accidents.

#### Compliance with ethical standards

**Conflicts of interest** The authors declare that they have no conflict of interest.

**Open Access** This article is distributed under the terms of the Creative Commons Attribution 4.0 International License (<http://creativecommons.org/licenses/by/4.0/>), which permits unrestricted use, distribution, and reproduction in any medium, provided you give appropriate credit to the original author(s) and the source, provide a link to the Creative Commons license, and indicate if changes were made.

#### References

1. Brach, R.M., Brach, R.M.: Vehicle Accident Analysis and Reconstruction Methods. SAE International, Pennsylvania (2005)
2. Brogliatto, B.: Non-smooth Mechanics. Springer, New York (2016)
3. Campbell, K.L.: Energy basis for collision severity. SAE Paper 740565 (1974)
4. Day, T.D.: An overview of the EDSMAC4 collision simulation model. SAE Paper 1999-01-0102 (1999)
5. Faik, S., Witteman, H.: Modeling of impact dynamics: a literature survey. In: Proceedings of International ADAMS User Conference (2000)
6. Gidlewski, M., Prochowski, L.: Analysis of motion of the body of a motor car hit on its side by another passenger car. In: IOP Conference Series: Materials Science and Engineering, vol. 148/2016, Paper No 012039



7. Gidlewski, M., Prochowski, L., Zielonka, K.: Analysis of the influence of motor cars' relative positions during a right-angle crash on the dynamic loads acting on car occupants and the resulting injuries, Paper No 15-0107, 24th ESV International Technical Conference, Gothenburg, Sweden [www.nhtsa.gov/ESV](http://www.nhtsa.gov/ESV) (2015)
8. Gillardi, G., Sharf, I.: Literature survey of contact dynamics modeling. *Mech. Mach. Theory* **37**, 1213–1239 (2002)
9. Happee, R., Janssen, A.J., Monster, J.W.: Application of MADYMO ossupant models in LS-DYNA/MADYMO coupling. In: 4th European LS-DYNA Users Conference, Ulm (2003)
10. Huang, M.: *Vehicle Crash Mechanics*. CRC Press LLC, Boca Raton (2002)
11. Jankowski, K.P., Gidlewski, M., Jemioł, L.: Comparative study of vehicle absorbed energy determination for road accident reconstruction, XVIIEVU Annual Meeting Kraków (2007)
12. Kitagawa, Y., Makita, M., Pal, C.: Evaluation and research of vehicle body stiffness and strength for car to car compatibility, SAE Paper No 2003-01-0908 (2003)
13. Kubiak, P., Siczek, K., Dabrowski, A., Szosland, A.: New high precision method for determining vehicle crash velocity based on measurements of body deformation. *Int. J. Crashworthiness* **21** (2016)
14. Kubiak, P.: Nonlinear approximation method of vehicle velocity  $V_t$  and statistical population of experimental cases. *Forensic Sci. Int.* **281**, 147–151 (2017)
15. McHenry, R.R., McHenry, B.G.: Effects of restitution in the application of crush coefficients. SAE Paper 970960 (1997)
16. National Highway Traffic Safety Administration Vehicle Crash Test Database, <https://www.nhtsa.gov/research-data/databases-and-software>, Test No. 3188, 3455, 3457, 4683
17. Nystrom, G.A.: Stiffness parameters for vehicle collision-analysis, an update. SAE Paper 2001-01-0502 (2001)
18. Pawlus, W., Karimi, H.R., Robbersmyr, K.G.: Investigation of vehicle crash modeling techniques: theory and application. *Int. J. Adv. Manuf. Technol.* **70**(5–6), (2014)
19. Prasad, A.K.: Energy absorbed by vehicle structures in side-impacts. SAE Paper No 910599 (1991)
20. Prasad, A.K.: Energy dissipated in vehicle crush—a study using the repeated test technique. SAE Paper No 900412 (1990)
21. Prochowski, L., Unarski, J., Wach, W., Wicher, J.: *Podstawy rekonstrukcji wypadków drogowych (Fundamentals of the reconstruction of road accidents)*, Wydawnictwa Komunikacji i Łączności, Warszawa (2014)
22. Rose, N.A., Fenton, S.J., Beauchamp, G.: Restitution modeling for crush analysis: theory and validation. SAE Paper 2006-01-0908 (2006)
23. Rose, N.A., Fenton, S.J., Ziernicki, R.M.: Crush and conservation of energy analysis: toward a consistent methodology. SAE Paper 2005-01-1200 (2005)
24. Schmorte, U.: Crash-test results to analyse the impact of non-professional repair on the performance of side structure of a car, Paper No 000310. In: 22nd ESV International Technical Conference (2011)
25. Schoenmakers, F.: MADYMO and LS\_DYNA the strenght of a combined approach. In: 7th European LS-DYNA Users Conference, Salzburg (2009)
26. Stewart, D.E.: Rigid-body dynamics with friction and impact. *SIAM Rev* **42**(1), 3–39 (2000)
27. Stronge, W.J.: *Impact Mechanics*. Cambridge University Press, Cambridge (2004)
28. Wach, W.: Calculation reliability in vehicle accident reconstruction. *Forensic Sci. Int.* **263**, 27–38 (2016)
29. Wach, W., Unarski, J.: Determination of vehicle velocities and collision location by means of monte carlo simulation method. SAE Technical Paper 2006-01-0907 (2006)
30. Ziubiński, M., Prochowski, L., Gidlewski, M.: Experimental and analytic determining of changes in motor cars positions in relation to each other during a crash test carried out to the FMVSS 214 procedure. In: 11th International Scientific and Technical Conference Automotive Safety, Slovakia (2018)
31. Zomotor, A.: *Fahrwerktechnik: Fahrverhalten*. Würzburg, Vogel (1991)
32. Żardecki, D.: Static friction indeterminacy problems and modeling of stick-slip phenomenon in discrete dynamic systems. *J. Theor. Appl. Mech.* **45**(2), 289–310 (2007)
33. Żuchowski, A.: The use of energy methods at the calculation of vehicle impact velocity. *Arch. Automot. Eng.* **68**(2), 85–111 (2015)